Electron-impact ionization of Pb^{q+} ions for $q=1-10$

S. D. Loch, J. A. Ludlow, and M. S. Pindzola
Department of Physics, Auburn University, Auburn, Alabama 36849, USA

F. Scheuermann, K. Kramer, B. Fabian, K. Huber, and E. Salzborn
Institut für Atom-und Molekülphysik, University of Giessen, D-35392 Giessen, Germany
(Received 27 May 2005; published 14 September 2005)

Theoretical calculations and experimental crossed-beam measurements are compared for electron-impact single ionization of Pb^{q+} ions for $q=1-10$. We compare with two main theoretical methods. First, we check against configuration-average distorted-wave calculations, which include both direct-ionization and indirect excitation-autoionization contributions. Second, for ion stages Pb^{+} through to Pb^{5+}, we calculate the dominant excitation-autoionization channels using level-resolved distorted-wave theory to evaluate the excitation cross sections. We find that for ion stages Pb^{+}, Pb^{2+}, and Pb^{3+}, distorted-wave theory significantly overestimates the total-ionization cross section, due to an overestimation of the direct-ionization cross section from the $5d$ subshell. For ion stages Pb^{4+} through to Pb^{10+} there is good agreement between theory and experiment. We find evidence for significant metastable fraction in the ion beam of the experiment for ion stages Pb^{2+}, Pb^{3+}, Pb^{4+}, Pb^{5+}, and Pb^{6+}. For ion stage Pb^{3+} we find that the level-resolved distorted-wave calculation of the excitation autoionization results in a slight reduction of the configuration-average theoretical results, due to splitting of levels within the autoionizing configurations. We also investigate two semiempirical methods of calculating the direct-ionization cross sections: namely, the Lotz method and the binary encounter Bethe method. We find that both methods provide results which are significantly lower than the distorted-wave method for the $5d$-subshell direct ionization of Pb^{+}, Pb^{2+}, and Pb^{3+}. For the higher ion stages, both methods are lower than the distorted-wave direct-ionization cross-section results, trending towards the distorted-wave results as the ion stage increases.

DOI: 10.1103/PhysRevA.72.032713 PACS number(s): 34.80.Dp, 52.20.Fs

I. INTRODUCTION

There is currently significant interest in the radiating properties of heavy species, such as tungsten, for use in magnetically confined fusion experiments. Such heavy species are being considered for use in plasma facing components and as wall erosion markers [1]. There have already been experiments and studies performed on tungsten, hafnium [2,3], and xenon. The interpretation of such experiments requires accurate electron-impact excitation, ionization, and recombination atomic data. For many of the ion stages observed in tokamak experiments, there are no experimental cross sections available. Thus, there is a need to assess the theoretical methods which are likely to be used to generate the atomic data for these heavy species. With this in mind, we compare measurements and theoretical calculations for the total electron-impact single-ionization cross section for Pb^{q+} ions for $q=1-10$, with Pb being an element of similar complexity to the expected tokamak elements of interest.

Our experimental measurements were taken at the Giessen electron-ion crossed-beam setup. To the best of the authors' knowledge the cross sections presented here are the first measurements of the electron-impact single-ionization cross sections of Pb ions. We compare these measurements primarily with the configuration-average distorted-wave (CADW) method [4], which was formulated to calculate electron-impact excitation, ionization, and recombination cross sections for complex atomic ions. The CADW method has been used successfully in calculations of the ionization cross sections for a range of complex species, such as Fe [5,6] and Mo [7]. Recently CADW calculations were performed on all ion stages of Kr [8] and on the first ten ion stages of Bi [9]. We also compare our CADW results for the direct ionization with two semiempirical methods: namely, the Lotz expression [10] and the binary encounter Bethe (BEB) method [11,12]. There has been one previous theoretical study on Pb by Povyshev *et al.* [13], which calculated the electron-impact single-ionization cross section for all ion stages of Pb, in the Coulomb-Born with exchange approximation.

One of our aims in this paper is to see which Pb ion stages can be described adequately with distorted-wave theoretical results and which ones cannot be described well and require perhaps a nonperturbative approach. We would also like to determine if there are any stages for which a configuration-average approach for the excitation autoionization is not sufficient, with a level-resolved calculation instead being required. In the CADW approach, the contribution to excitation autoionization for a particular configuration is either all included or all excluded, depending upon whether the excitation energy is above or below the ionization threshold. It may be the case that level splitting of a configuration which lies just above the ionization threshold results in levels which are in fact bound. Conversely, a configuration which lies below the ionization threshold could be level split such that some of its levels lie above the ionization threshold. For this reason we have performed level-resolved distorted-wave excitation cross-section calculations on selected transitions.

From past experience, we can predict the likely trends of the distorted-wave direct and indirect cross-section compari-

sons with experiment. First, we do not expect the DW methods to produce good agreement for the near-neutral stages. Considering the direct-ionization cross section for near neutrals, it has been seen frequently that distorted-wave methods overestimate the direct-ionization cross section—for example, in W [14], Mo [7], Kr [8], and Bi [9]. This is because the distorted-wave method includes the full three-body Coulomb interaction only through first-order perturbation theory. It has been previously seen that nonperturbative approaches (e.g., the time-dependent close-coupling method) can produce significantly reduced cross sections, compared with distorted-wave theory for near-neutral systems—e.g., the cases of He [15], Li [16], and C^{2+} [17]. We might also expect the distorted-wave method to overestimate the excitation cross sections for near-neutral systems, as has been seen in Sc^{+} [18] and Sc^{2+} [19] where nonperturbative calculations of the excitation autoionization produced smaller cross-section results, compared with the distorted-wave results. However, for complex species such as Pb, nonperturbative calculations are extremely demanding, and perturbative approaches such as distorted-wave or semiempirical methods are currently the only option. So we would expect distorted-wave methods to overestimate the total-ionization cross section for the near-neutral ion stages of Pb. However, for stages more than a few times ionized, the distorted-wave method should give reasonably accurate results. As the *d* subshell becomes progressively less filled, with a corresponding increase in the number of associated terms, one would expect the configuration-average method to be a good representation of the ionizing configuration. With the large number of terms in the ground configuration, it is likely that any metastable terms are associated with the ground configuration, again implying that the configuration-average method should give good agreement with experiment, as it will account for the metastable presence as well. Good agreement between experiment and distorted-wave theory, for ionized systems, has been seen many times—for example, in Kr [8] and Bi [9].

The rest of this paper is outlined as follows. In Sec. II we describe the theoretical methods used in the paper, Sec. III describes the experimental setup, Sec. IV compares the experimental and theoretical results, and in Sec. V we summarize our results.

II. THEORY

The main contributions to the electron-impact single-ionization cross section are from direct ionization

$$e^- + \mathrm{Pb}^{q+} \rightarrow \mathrm{Pb}^{(q+1)+} + e^- + e^- \tag{1}$$

and excitation autoionization

$$e^- + \mathrm{Pb}^{q+} \rightarrow (\mathrm{Pb}^{q+})^* + e^- \rightarrow \mathrm{Pb}^{(q+1)+} + e^- + e^-. \tag{2}$$

Here q is the initial charge of the ion, $(\mathrm{Pb}^{q+})^*$ represents an excited state of the ion, and for the process of excitation autoionization, there is also the possibility of radiative stabilization occurring before the excited ion can autoionize. Thus, autoionizing configurations are associated with an Auger yield, giving the fraction of electrons that will autoionize from such a configuration.

Thus, the total cross section, considering both direct and indirect (i.e., excitation-autoionization) processes, is

$$\sigma_{total} = \sum_i \sigma_{direct} + \sum_j \sigma_{indirect}, \tag{3}$$

where the sum i is over the direct ionization channels and the sum j is over the inner subshell electrons which can be excited, leading to an autoionizing configuration. We calculate the direct-ionization cross section primarily using a configuration-average distorted-wave method [4]. The indirect excitation-autoionization contribution to the total ionization cross section is given by

$$\sigma_{indirect}(j) = \sum_k \sigma_{exc}(j \rightarrow k) B_k^a, \tag{4}$$

where $\sigma_{exc}(j \rightarrow k)$ is the excitation cross section from a level j of the initial configuration to a level k of the final excited configuration. The branching ratio for autoionization, B_k^a, from level k is the ratio of the total Auger rate to the total Auger and radiative rates from level k. For all of the ion stages presented here the autoionization rates will be far greater than the radiative rates and the branching ratios are unity. One would not expect the radiative rates to reduce the branching ratios until much higher ion stages. In the work presented here, the electron-impact excitation cross sections are calculated using a configuration-average distorted-wave method [4] or a level-to-level distorted-wave method [20].

A. Direct ionization

The direct-ionization process can be evaluated using the configuration-average distorted-wave method [4] representing the transition

$$(nl)^{\omega} k_i l_i \rightarrow (nl)^{\omega-1} k_e l_e k_f l_f, \tag{5}$$

where ω is the occupation number of the initial subshell being ionized and $k_i l_i$ are the quantum numbers of the incident electron, while $k_e l_e$ and $k_f l_f$ are the quantum numbers for the ejected and final continuum electrons, respectively. The configuration-average direct cross section is given by

$$\sigma = \frac{32\omega}{k_i^3} \int_0^{E/2} \frac{d(k_e^2/2)}{k_e k_f} \sum_{l_i, l_e, l_f} (2l_i + 1)(2l_e + 1) \times (2l_f + 1) P(l_i, l_e, l_f, k_i, k_e, k_f), \tag{6}$$

where P is the first-order scattering probability and has been described in more detail previously [4].

There are commonly two different approximations made for the scattering potential which the incident, scattered, and ejected electrons experience. In what will be referred to as the distorted wave incident and scattered (N) or DWIS(N) method, the incident and scattered electrons are evaluated in a V^N potential, with the ejected continuum electron calculated in a V^{N-1} potential, where N is the number of electrons in the initial target. Alternatively one can calculate the incident, scattered, and ejected electrons in a V^{N-1} potential, labeled as DWIS($N-1$).

There are many semiempirical methods for calculating the direct-ionization cross section, such as the Lotz method [10]

or the BEB method [11,12], to name just two which are commonly used. In this paper we investigate the effectiveness of the Lotz and BEB methods in calculating the direct ionization for these Pb ions. The Lotz expression [10] is a semiempirical method, where the total-ionization cross section (cm^2) from subshells k with occupation number ξ_k and ionization potential I_k (eV), as a function of incident electron energy ε (eV), is given by

$$\sigma(\varepsilon) = 4.5 \times 10^{-14} \sum_k \xi_k \frac{\ln(\varepsilon/I_k)}{\varepsilon I_k}. \tag{7}$$

The BEB model [11,12] is calculated via the equation

$$\sigma_{ion} = \frac{4\pi a_0^2 \omega R^2}{B^2[t+(u+1)/n]} \left[\frac{\ln t}{2}\left(1-\frac{1}{t^2}\right) + \left(1-\frac{1}{t}\right) - \frac{\ln t}{t+1} \right], \tag{8}$$

where ω is the occupation number of the subshell being ionized, a_0 is the Bohr radius, R is the Rydberg unit of energy (13.61 eV), $u=U/B$, and $t=T/B$ where T, U, and B are the incident electron energy, the bound electron's kinetic energy, and binding energy, respectively. n is a refinement on the method first reported in [11] and is the principal quantum number of the shell being ionized and is set to 1 for $n<3$.

B. Configuration-average excitation

In this paper our default method for calculating the excitation cross section is the configuration-average distorted-wave method [4]. As a refinement on this method we can calculate level-resolved distorted-wave excitation cross sections for the dominant, or the near-threshold, excitation cross sections which participate in excitation autoionization. The configuration-average approach is considerably simpler than the level-resolved method. In the configuration-average approach, the excitation process is represented by

$$(n_1 l_1)^{\omega_1+1}(n_2 l_2)^{\omega_2-1} k_i l_i \rightarrow (n_1 l_1)^{\omega_1}(n_2 l_2)^{\omega_2} k_f l_f, \tag{9}$$

where $n_1 l_1$ and $n_2 l_2$ are quantum numbers of the bound electrons and $k_i l_i$ and $k_f l_f$ are quantum numbers of the initial and final continuum electrons, respectively. The configuration-average excitation cross section is given by

$$\sigma_{exc} = \frac{8\pi}{k_i^3 k_f}(\omega_1+1)(4l_2+3-\omega_2)\sum_{l_i,l_f}(2l_i+1) \times (2l_f+1)P(l_i,l_f,k_i,k_f), \tag{10}$$

where P is the first-order scattering probability [4].

C. Level-resolved excitation

The most general excitation transition between levels is of the form

$$(\alpha_i J_i) k_i l_i j_i J \rightarrow (\alpha_f J_f) k_f l_f j_f J, \tag{11}$$

where J_i is the total angular momentum for the target bound state, α_i represents all other quantum numbers needed to specify the intermediate-coupled target bound state, J is the total angular momentum of the electron-ion system, and $k_i l_i j_i$ and $k_f l_f j_f$ are the quantum numbers of the incident and final continuum electrons, respectively. The level-to-level excitation cross section is given by

$$\sigma_{exc}(i \rightarrow f) = \frac{4\pi}{k_i^3 k_f} \frac{1}{2(2J_i+1)} \sum_{l_i j_i} \sum_{l_f j_f} \sum_J (2J+1) \times |T(\alpha_i J_i k_i l_i j_i J \rightarrow \alpha_f J_f k_f l_f j_f J)|^2, \tag{12}$$

where the T matrix has been described in detail previously [20]. The energies and orbitals required to calculate the level-resolved distorted-wave excitation cross sections (LRDW) are evaluated in the Hartree-Fock relativistic (HFR) approximation.

III. EXPERIMENTAL SETUP

The measurements were performed at the Giessen electron-ion crossed-beam setup. A detailed description can be found in Tinschert *et al.* [21] and Hofmann *et al.* [22]. The Pb^{q+} ions were produced by evaporating lead from an oven into the plasma of a 14-GHz electron cyclotron resonance (ECR) ion source (Brötz [23]). The desired mass-to-charge ratio was selected using a magnetic field. After tight collimation to typically 1 mm diameter the ion beam was crossed with an intense electron beam. For charge-state Pb^{10+} ions we obtained about 3 nA; for lower-charge states, higher currents could be obtained. The acceleration voltage used is 10 kV. The ionization products were separated from the incident ion beam after the interaction using a magnetic field. They were detected by a single-particle detector, while a large Faraday cup collected the primary ion beam.

To obtain absolute cross sections, the dynamic crossed-beam technique (Müller *et al.* [24]) was employed. There the electron gun—i.e., the electron beam—is moved up and down across the ion beam with simultaneous registration of the ionization signal, the electron, and the ion current. The electron gun we used was designed by Becker *et al.* [25] and delivers an electron current of up to 430 mA at the maximum energy of 1 keV. The typical measurement time is about 40 s for high cross sections at high energies and up to 2000 s near threshold. The total experimental uncertainties of the measured cross sections are typically 8% at the maximum resulting from the quadrature sum of the nonstatistical errors of about 7.8% and the statistical error at 95% confidence level.

IV. RESULTS

A. Pb^+

The theoretical and experimental results for Pb^+ are shown in Fig. 1. Pb^+ has a ground configuration of $5d^{10}6s^26p$. The configuration-average results include direct ionization from the $6p$, $6s$, and $5d$ subshells. Ionization from the $5p$, $5s$, and $4f$ subshells lies above the double-ionization threshold (44.58 eV) and thus has not been included in the theoretical results. We also include the effects of excitation autoionization via excitation from the $6s$ subshell to the $5d^{10}6s6pnl$ configurations and excitation from the $5d$ subshell to the $5d^96s^26pnl$ configurations, where $5 \leqslant n \leqslant 8$ and

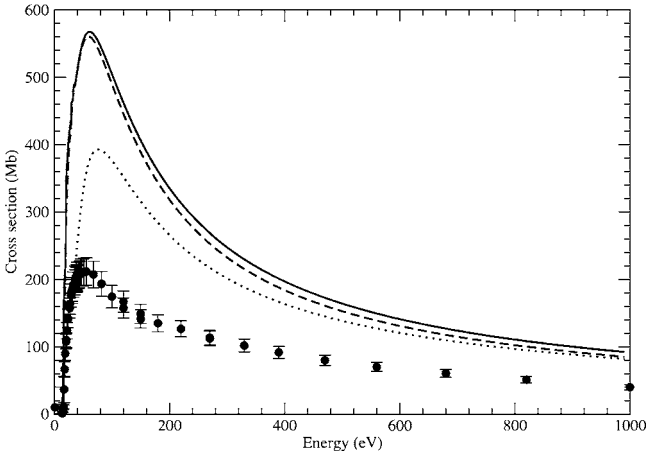

FIG. 1. Electron-impact single-ionization cross section for Pb^+, which has a ground configuration of $5d^{10}6s^26p$. The dotted line gives the total configuration-average distorted-wave direct-ionization (CADW-DI) cross section, and the solid line gives the total CADW-DI plus the total configuration-average distorted-wave excitation-autoionization (CADW-EA) cross section. The dashed curve shows the total CADW-DI results, along with level-resolved distorted-wave results for the dominant excitation-autoionization channels ($5d \rightarrow 6p$, $6s \rightarrow 6d$, $7s$ and $7p$), with the remaining excitation-autoionization channels being calculated using the CADW method. The solid circles show the current experimental measurements.

$0 \leqslant l \leqslant 3$. Table I shows the direct ionization potentials for Pb^+.

The theory results clearly overestimate the total-ionization cross section. Just the direct-ionization cross section by itself is already significantly above the experimental measurements. It appears that the distorted-wave method is overestimating the direct-ionization cross section for such a near-neutral species. This has already been seen in various systems (e.g., Kr [8], Mo [7], Bi [9]) and is not unexpected. It may be that a nonperturbative calculation would provide a more accurate calculation for the direct ionization. This is currently under investigation. In order to see if the excitation-autoionization calculation could be improved, we performed level-resolved distorted-wave calculations for the dominant excitation-autoionization channels ($5d \rightarrow 6p$ and $6s \rightarrow 6d$, $7s$, and $7p$). The results are shown by the dashed curve in Fig. 1. It can be seen that the level-resolved results are very close to the CADW results, since very few of the levels actually straddle the ionization threshold. Note that it is also possible that the distorted-wave method is overestimating the excitation cross sections for the excitation-autoionization contribution.

The CADW direct-ionization results shown here, and for all other ion stages, are for the DWIS($N-1$) method. We also calculated the DWIS(N) results and found that the differences between DWIS(N) and DWIS($N-1$) were small. The differences have a maximum of about 5% at the peak of the cross section, with both methods coming into agreement at higher energy. One exception is for the case of Pb^{3+}, where the DWIS(N) direct-ionization cross section peaks near 130 Mb, instead, compared with about 105 Mb for the DWIS($N-1$) cross section. In order to keep the figures clear, we do not show the DWIS(N) for Pb^+ or for any of the other ion stages.

Note that we will discuss semiempirical methods of calculating the direct-ionization cross section for all ion stages in Sec. IV K. Thus, we will comment on the Lotz and BEB results for Pb^+, and all other ion stages, in that section, where we look at trends along the isonuclear sequence.

B. Pb^{2+}

The theoretical and experimental results for Pb^{2+} are shown in Figs. 2 and 3. Pb^{2+} has a ground configuration of $5d^{10}6s^2$. Direct ionization from the $6s$ and $5d$ subshells is included, as well as excitation autoionization via the $5d$ subshell to the $5d^96s^2nl$ configurations, where $5 \leqslant n \leqslant 8$ and $0 \leqslant l \leqslant 3$. Note that excitation of the $5p$ subshell leads to configurations above the double-ionization threshold and has thus been omitted in the theoretical results shown. Table I shows the direct-ionization potentials for the ground and first excited configurations of Pb^{2+}.

It can be seen that the basic CADW results lie significantly higher than experiment, though the level of disagreement is less than that for the Pb^+ case. Again it is the case that the distorted-wave theoretical results for the direct-ionization cross section alone lie above experiment. It is likely that the distorted-wave theoretical results for direct ionization are overestimating the cross section, since it treats the three-body continuum interaction in only first-order perturbation theory. We performed level-resolved distorted-wave calculations for the dominant excitation-autoionization channels ($5d \rightarrow 5f$, $6d$ and $6f$), with the results being essentially the same results as for the CADW method; see the dashed curve in Fig. 2. We note that all of the distorted-wave results are coming into agreement with experiment at higher energy, near 800 eV.

There is clearly a metastable fraction present in the experiment, with an ionization contribution opening up at about 12 eV and then again at about 21 eV. The metastable at 12 eV is, as yet, unidentified. The contribution at 21 eV is likely to be from the $5d^{10}6s6p$ configuration, due to the long lifetime of the ^3P term. From Fig. 3 one can see that the ionization cross section for the $5d^{10}6s6p$ configuration agrees in both position and shape with the increase in the experimental cross section near 21 eV. The identity of the metastable which is contributing close to 12 eV is not so clear. It may be the $5d^{10}6p^2$ configuration, since the threshold is close to the right energy, but one would think that this would decay to the $5d^{10}6s6p$ configuration.

C. Pb^{3+}

The theoretical and experimental results for Pb^{3+} are shown in Figs. 4 and 5. Pb^{3+} has a ground configuration of $5d^{10}6s$. Table I shows the direct-ionization potentials for the ground and first excited configurations of Pb^{3+}. We include direct ionization from the $6s$ and $5d$ subshells. We include indirect ionization via core excitation of the $5d$ subshells into the $5d^96snl$ configurations, where $5 \leqslant n \leqslant 8$ and $0 \leqslant l \leqslant 3$. Again, the theoretical results are significantly higher than the

TABLE I. Configuration-average ionization potentials for the subshells in the ground and selected excited configurations for Pb^{+} through to Pb^{10+}; the configuration-average double ionization potentials are also shown.

Ion stage	Double IP (eV)	Transition			IP (eV)
Pb^{+}	44.58	$5d^{10}6s^{2}6p$	→	$5d^{10}6s^{2}$	13.94
			→	$5d^{10}6s6p$	22.66
			→	$5d^{9}6s^{2}6p$	35.60
Pb^{2+}	72.01	$5p^{6}5d^{10}6s^{2}$	→	$5p^{6}5d^{10}6s$	30.64
			→	$5p^{6}5d^{9}6s^{2}$	45.14
			→	$5p^{5}5d^{10}6s^{2}$	119.32
Pb^{2+}	72.01	$5p^{6}5d^{10}6s6p$	→	$5p^{6}5d^{10}6s$	21.92
			→	$5p^{6}5d^{10}6p$	32.82
			→	$5p^{5}5d^{9}6s6p$	46.67
Pb^{3+}	110.77	$5p^{6}5d^{10}6s$	→	$5p^{6}5d^{10}$	41.37
			→	$5p^{6}5d^{9}6s$	56.95
			→	$5p^{5}5d^{10}6s$	131.47
Pb^{3+}	110.77	$5p^{6}5d^{9}6s6p$	→	$5p^{6}5d^{9}6s$	32.20
			→	$5p^{6}5d^{9}6p$	44.63
			→	$5p^{6}5d^{8}6s6p$	62.07
Pb^{4+}	155.72	$4f^{14}5s^{2}5p^{6}5d^{10}$	→	$4f^{14}5s^{2}5p^{6}5d^{9}$	69.40
			→	$4f^{14}5s^{2}5p^{5}5d^{10}$	144.31
			→	$4f^{14}5s5p^{6}5d^{10}$	205.40
			→	$4f^{13}5s^{2}5p^{6}5d^{10}$	190.31
Pb^{4+}	155.72	$5s^{2}5p^{6}5d^{9}6s$	→	$5s^{2}5p^{6}5d^{9}$	53.82
			→	$5s^{2}5p^{6}5d^{8}6s$	73.19
			→	$5s^{2}5p^{5}5d^{9}6s$	148.31
			→	$5s5p^{6}5d^{9}6s$	210.27
Pb^{5+}	190.27	$4f^{14}5s^{2}5p^{6}5d^{9}$	→	$4f^{14}5s^{2}5p^{6}5d^{8}$	86.31
			→	$4f^{14}5s^{2}5p^{5}5d^{9}$	161.85
			→	$4f^{14}5s5p^{6}5d^{9}$	223.71
			→	$4f^{13}5s^{2}5p^{6}5d^{9}$	209.70
Pb^{5+}	190.27	$5s^{2}5p^{6}5d^{8}6s$	→	$5s^{2}5p^{6}5d^{8}$	66.95
			→	$5s^{2}5p^{6}5d^{7}6s$	90.21
			→	$5s^{2}5p^{5}5d^{8}6s$	165.91
			→	$5s5p^{6}5d^{8}6s$	228.70
Pb^{6+}	226.20	$4f^{14}5s^{2}5p^{6}5d^{8}$	→	$4f^{14}5s^{2}5p^{6}5d^{7}$	103.95
			→	$4f^{14}5s^{2}5p^{5}5d^{8}$	180.06
			→	$4f^{14}5s5p^{6}5d^{8}$	242.79
			→	$4f^{13}5s^{2}5p^{6}5d^{8}$	230.06
Pb^{6+}	226.20	$4f^{14}5s^{2}5p^{6}5d^{7}6s$	→	$4f^{14}5s^{2}5p^{6}5d^{7}$	80.69
			→	$4f^{14}5s^{2}5p^{6}5d^{6}6s$	107.94
			→	$4f^{14}5s^{2}5p^{5}5d^{7}6s$	184.20
			→	$4f^{14}5s5p^{6}5d^{7}6s$	247.86
Pb^{7+}	263.43	$4f^{14}5s^{2}5p^{6}5d^{7}$	→	$4f^{14}5s^{2}5p^{6}5d^{6}$	122.25
			→	$4f^{14}5s^{2}5p^{5}5d^{7}$	198.96
			→	$4f^{14}5s5p^{6}5d^{7}$	262.56
			→	$4f^{13}5s^{2}5p^{6}5d^{7}$	251.30
Pb^{8+}	301.87	$4f^{14}5s^{2}5p^{6}5d^{6}$	→	$4f^{14}5s^{2}5p^{6}5d^{5}$	141.18
			→	$4f^{14}5s^{2}5p^{5}5d^{6}$	218.45
			→	$4f^{14}5s5p^{6}5d^{6}$	282.98
			→	$4f^{13}5s^{2}5p^{6}5d^{6}$	273.40

TABLE I. (*Continued.*)

Ion stage	Double IP (eV)	Transition			IP (eV)
Pb^{9+}	341.72	$4f^{14}5s^25p^65d^5$	→	$4f^{14}5s^25p^65d^4$	160.69
			→	$4f^{14}5s^25p^55d^5$	238.49
			→	$4f^{14}5s5p^65d^5$	304.00
			→	$4f^{13}5s^25p^65d^5$	296.29
Pb^{10+}	382.14	$4f^{14}5s^25p^65d^4$	→	$4f^{14}5s^25p^65d^3$	180.76
			→	$4f^{14}5s^25p^55d^4$	259.07
			→	$4f^{14}5s5p^65d^4$	325.60
			→	$4f^{13}5s^25p^65d^4$	319.96

experiment, with the results for the direct ionization alone lying close to the experimental measurements. We performed a level-resolved distorted-wave calculation for the dominant excitation-autoionization channels ($5d \rightarrow 5f, 6f$) and found a slight reduction in the total cross section, due to level splitting pushing levels below the ionization threshold. However, the reduction was not enough to bring theory into agreement with experiment. Again, it is likely that distorted-wave theory, which is treating the three-body continuum interaction in only a first-order perturbation theory approach, is not appropriate in this case.

The experiment has a significant cross section below the ionization threshold of the ground configuration, indicating the presence of metastable fraction in the beam; see Fig. 5. The experimental threshold agrees with that for the $5d^96s6p$ excited configuration. Thus, we calculated CADW direct ionization for this excited configuration, allowing for direct ionization from the $6p$, $6s$, and $5d$ subshells. We also included CADW excitation autoionization via excitation of a $6s$ electron into the $5d^96pnl$ configurations and of a $5d$ electron into the $5d^86s6pnl$ configurations, where $5 \leqslant n \leqslant 8$ and $0 \leqslant l \leqslant 3$. The metastable total-ionization cross section is close in height to that from the ground configuration; thus, a mixture of the ground and first excited configurations still cannot be found that would produce agreement with experiment. From the below-threshold ionization, metastable presence seems likely, and the disagreement between theory and experiment is probably due to distorted-wave theory overestimating the direct-ionization cross section.

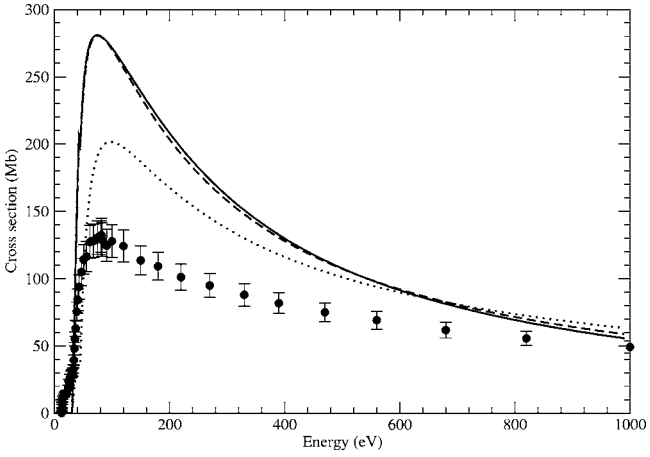

FIG. 2. Electron-impact single-ionization cross section for Pb^{2+}, which has a ground configuration of $5d^{10}6s^2$. All theory results shown are for the ground configuration. The dotted line gives the total CADW-DI cross section, and the solid line gives the total CADW-DI plus the total CADW-EA cross section. The dashed curve shows the total CADW-DI results, along with level-resolved distorted-wave results for the dominant excitation-autoionization channels ($5d \rightarrow 5f$, $6d$ and $6f$), with the remaining excitation-autoionization channels being calculated using the CADW method. The solid circles show the current experimental measurements.

D. Pb^{4+}

The theoretical and experimental results for Pb^{4+} are shown in Fig. 6. Pb^{4+} has a ground configuration of $5d^{10}$. Thus, one would expect there to be possible metastable fraction in the $5d^96s$ configuration, especially the ^3D term associated with that configuration. Table I shows the direct-

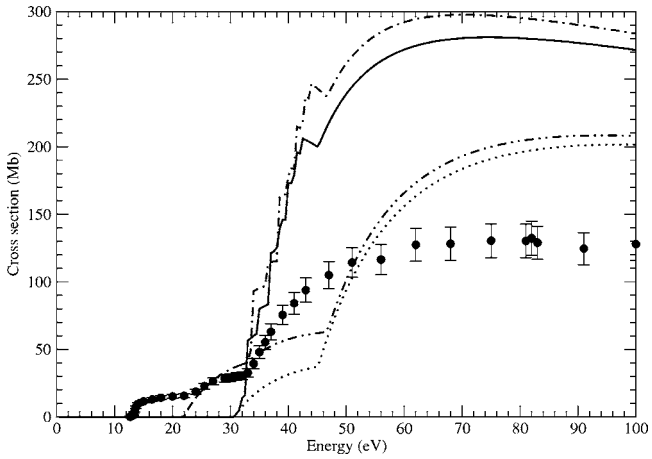

FIG. 3. Electron-impact single-ionization cross section for Pb^{2+} in the low-energy region. Pb^{2+} has a ground configuration of $5d^{10}6s^2$ and potential metastable in the excited $5d^{10}6s6p$ configuration. The dotted line gives the total CADW-DI results for the ground configuration. The solid line gives the total CADW-DI plus the total CADW-EA cross section, again for the ground configuration. The double-dot–dashed results show the total CADW-DI results for the $5d^{10}6s6p$ excited configuration. The dot-dashed results show the total CADW-DI results plus the total CADW-EA for the $5d^{10}6s6p$ excited configuration. The solid circles show the current experimental measurements.

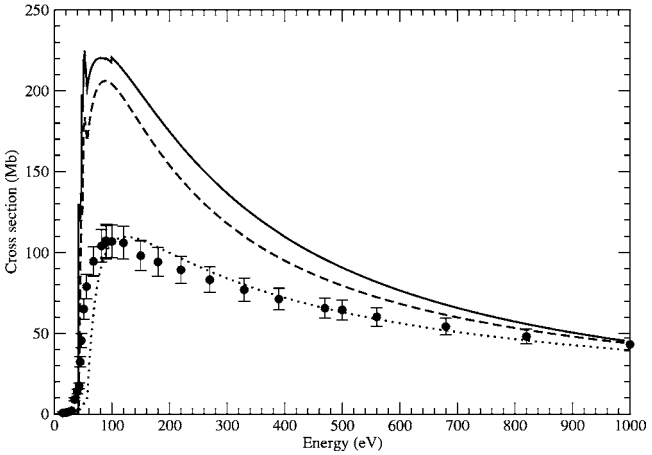

FIG. 4. Electron-impact single-ionization cross section for Pb^{3+}, which has a ground configuration of $5d^{10}6s$. All theory results shown are for the ground configuration. The dotted line gives the total CADW-DI results, and the solid line gives the total CADW-DI plus the total CADW-EA cross section. The dashed curve shows the total CADW-DI results, along with level-resolved distorted-wave results for the dominant excitation-autoionization channels ($5d \rightarrow 5f, 6f$), with the remaining excitation-autoionization channels being calculated using the CADW method. The solid circles show the current experimental measurements.

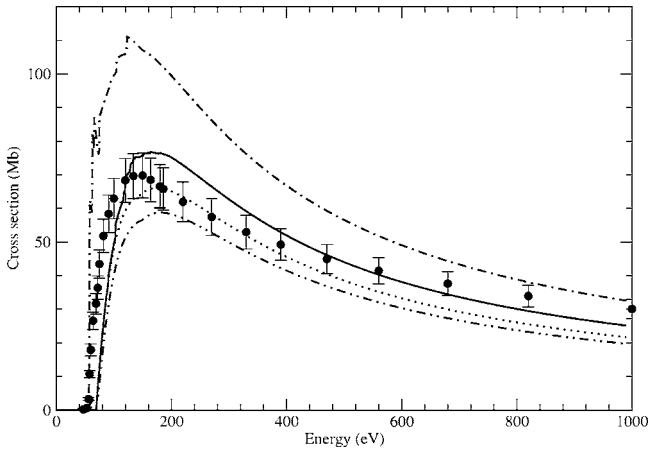

FIG. 6. Electron-impact single-ionization cross section for Pb^{4+}, which has a ground configuration of $5d^{10}$ and potential metastable in the $5d^9 6s$ configuration. The dotted line gives the total CADW-DI cross section from the ground configuration, and the solid line gives the total CADW-DI plus the total CADW-EA cross section for the ground configuration. The double-dot–dashed line gives the total CADW-DI cross section from the $5d^9 6s$ first excited configuration, and the dot-dashed line gives the total CADW-DI plus the total CADW-EA cross section for the first excited configuration. The solid circles show the experimental results.

ionization potentials for the ground and first excited configurations of Pb^{4+}.

In our theory results for the ground configuration we include direct ionization of the $5d$ and $5p$ subshells and excitation autoionization from the $5p$ subshell into the $5p^5 5d^{10} nl$ configurations, where $5 \leqslant n \leqslant 8$ and $0 \leqslant l \leqslant 3$. For the first excited configuration we include direct ionization of the $6s$, $5d$, and $5p$ subshells and excitation autoionization from the $5d$ and $5p$ subshells into the $5d^8 6snl$ and $5p^5 5d^9 6snl$ configurations, where $5 \leqslant n \leqslant 8$ and $0 \leqslant l \leqslant 3$.

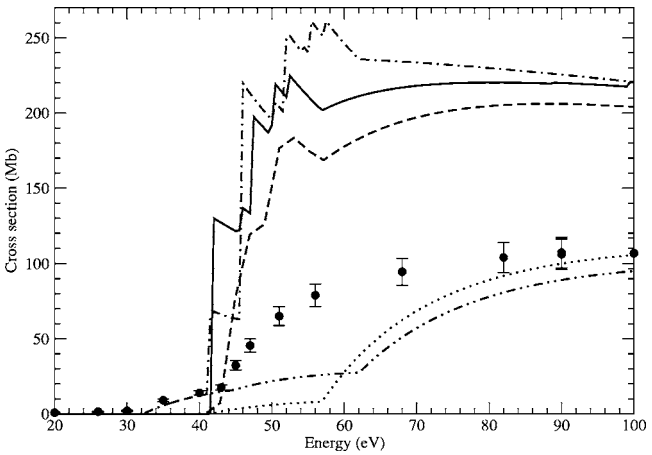

FIG. 5. Electron-impact single-ionization cross section for Pb^{3+} in the low-energy region. Pb^{3+} has a ground configuration of $5d^{10}6s$ and potential metastable in the excited $5d^9 6s6p$ configuration. For the ground configuration, the dotted line gives the total CADW-DI results and the solid line gives the total CADW-DI plus the total CADW-EA cross section. The dashed curve shows the total CADW-DI results, along with level-resolved distorted-wave results for the dominant excitation-autoionization channels ($5d \rightarrow 5f, 6f$), with the remaining excitation-autoionization channels being calculated using the CADW method. For the $5d^9 6s6p$ excited configuration, the double-dot–dashed line gives the total CADW-DI results and the dot-dashed line gives the total CADW-DI plus the total CADW-EA cross section.

From Fig. 6 one can see that there is a small amount of cross section below the theoretical ionization threshold for the ground configuration. The onset of the experimentally measured cross section agrees well with the theory results for the onset of the ionization of the $5d^9 6s$ first excited configuration. Reasonable agreement between theory and experiment in the threshold region would be achieved if a 30% metastable fraction is assumed. Note that even with a mixture of ground and metastable configurations, theory will still overestimate the total cross section near the peak of the cross section. However, the level of agreement in this case is much better than for the lower ion stages. It would appear that by Pb^{4+}, the DW method is becoming a reasonable method to calculate the ionization cross sections. Note that for the ground configuration of Pb^{4+} we also calculated LRDW excitation cross sections for the dominant excitations: namely, $5d \rightarrow 6f$, $7d$, and $7f$. There was no significant difference between these results and those of the CADW calculations; thus, in Fig. 6 we show only the CADW results.

E. Pb^{5+}

The theoretical and experimental results for Pb^{5+} are shown in Fig. 7. Pb^{5+} has a ground configuration of $5d^9$, which has only one term ^2D. Thus, the presence of metastable terms within the first excited configuration ($5d^8 6s$) is a strong possibility. We calculated CADW cross sections for

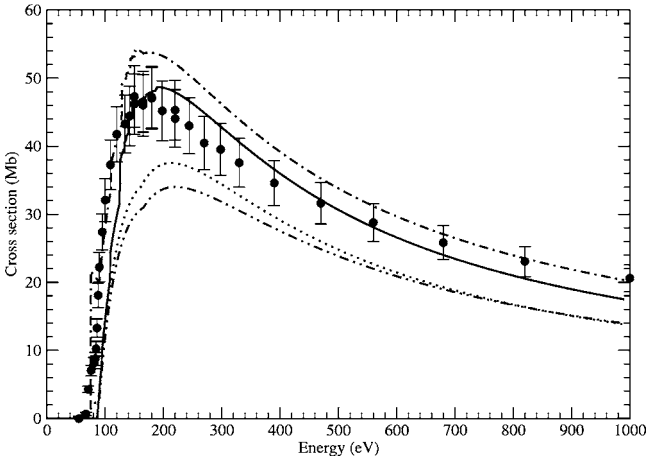

FIG. 7. Electron-impact single-ionization cross section for Pb^{5+}, which has a ground configuration of $5d^9$ and potential metastable in the $5d^86s$ first excited configuration. The dotted line gives the total CADW-DI cross section from the ground configuration, and the solid line gives the total CADW-DI plus the total CADW-EA cross section for the ground configuration. The double-dot–dashed line gives the total CADW-DI cross section from the $5d^86s$ first excited configuration, and the dot-dashed line gives the total CADW-DI plus the total CADW-EA cross section for the first excited configuration. The solid circles show the experimental results.

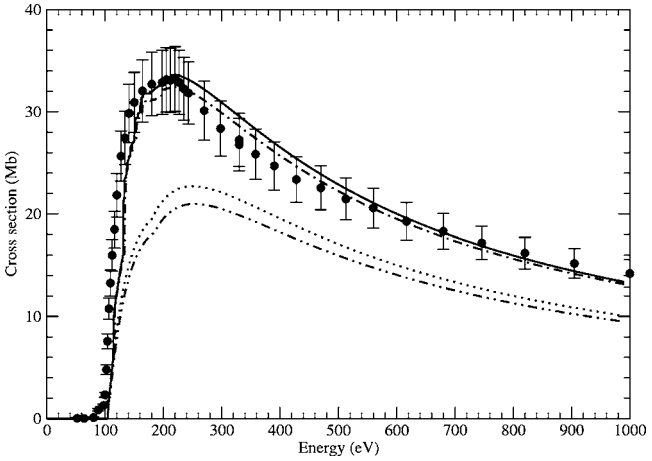

FIG. 8. Electron-impact single-ionization cross section for Pb^{6+}, which has a ground configuration of $5d^8$ and potential metastable in the $5d^76s$ first excited configuration. The dotted line gives the total CADW-DI cross section from the ground configuration, and the solid line gives the total CADW-DI plus the total CADW-EA cross section for the ground configuration. The double-dot–dashed line gives the total CADW-DI cross section from the $5d^76s$ first excited configuration, and the dot-dashed line gives the total CADW-DI plus the total CADW-EA cross section for the first excited configuration. The solid circles show the experimental results.

the ground configuration and the first excited configuration. Table I shows the direct-ionization potentials for Pb^{5+}.

From Fig. 7 it can be seen that there is clearly significant measured cross section below the threshold of ionization for the ground configuration and that it agrees with the threshold for the first excited configuration. The CADW results for the first excited configuration lie slightly above the measured results, while the CADW results for the ground configuration lie slightly below the measured values, suggesting that a mixture of metastables and ground-state ions is present in the experiment. The total cross sections for the ground and first excited configurations are very close to each other, making an estimation of the metastable fraction difficult. For the ground configuration we also calculated the dominant excitations, which are close to the threshold $(5p \rightarrow 6s, 6p)$, using the LRDW method. In the CADW picture, the excitation from the $5p$ subshell to the $6s$ subshell lies just below the ionization threshold and excitation from the $5p$ subshell to the $6p$ subshell lies just above the ionization threshold. We found that the LRDW results for the $5p \rightarrow 6p$ transition were essentially the same as the CADW results. Level splitting of the $5p \rightarrow 6s$ transition does lead to levels which are above the ionization threshold; however, it only contributes about 0.5 Mb to the total cross section. Thus, including our LRDW results does not make a significant difference to the CADW results, and we show only the CADW results in Fig. 7.

F. Pb^{6+}

The theoretical and experimental results for Pb^{6+} are shown in Fig. 8. Pb^{6+} has a ground configuration of $5d^8$, with terms ^1D, ^3F, ^3P, ^1G, and ^1S. We calculate the direct ionization from the $5d$ and $5p$ subshells and excitation autoionization from the $5p$ subshell via the $5p^55d^8nl$ configurations, where $5 \leqslant n \leqslant 8$ and $0 \leqslant l \leqslant 3$. We also calculate the ionization cross section from the $5d^76s$ configuration, to check for metastable presence. This excited configuration does have a couple of quintet terms, which could be metastable. In our total cross section for the first excited configuration we include the direct ionization of the $6s$, $5d$, and $5p$ subshells and excitation autoionization from the $5p$ and $5s$ subshells to the $5p^55d^86snl$ and $5s5p^65d^86snl$ configurations, respectively, where $5 \leqslant n \leqslant 8$ and $0 \leqslant l \leqslant 3$. Note that excitation from the $5d$ subshell does not lead to configurations which are autoionizing. Table I shows the direct-ionization potentials for Pb^{6+}. One can see from Fig. 8 that there is some measured cross section below the threshold for ionization of the ground configuration and that it lines up with the onset for ionization from the first excited configuration. At energies above the peak of the cross section the results from the ground and first excited configurations are quite similar. Again, the total cross sections for the ground and first excited configurations are quite similar, making estimation of a metastable fraction difficult.

We note that for Pb^{6+} and higher ion stages, the number of levels in the autoionizing configurations becomes very large, making calculation of level-resolved excitation cross sections to these levels prohibitive. Thus, for Pb^{6+} and for all higher ion stages, we show only the CADW results.

G. Pb^{7+}

The theoretical and experimental results for Pb^{7+} are shown in Fig. 9. Pb^{7+} has a ground configuration of $5d^7$. We include direct ionization of the $5d$, $5p$, $5s$, and $4f$ subshells

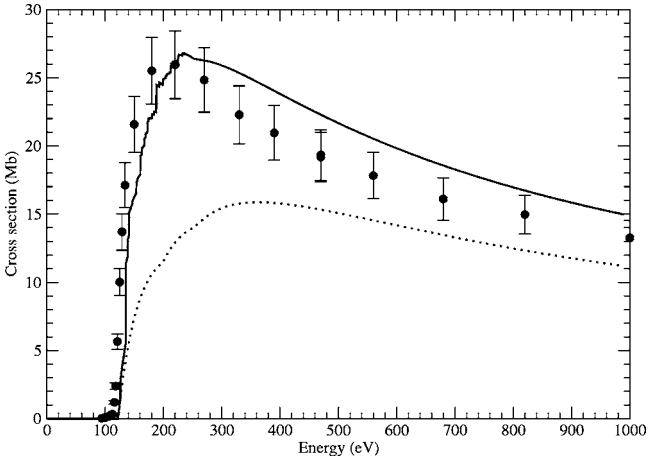

FIG. 9. Electron-impact single-ionization cross section for Pb^{7+}, which has a ground configuration of $5d^7$. The dotted line gives the total CADW-DI cross section from the ground configuration, and the solid line gives the total CADW-DI plus the total CADW-EA cross section for the ground configuration. The solid circles show the experimental results.

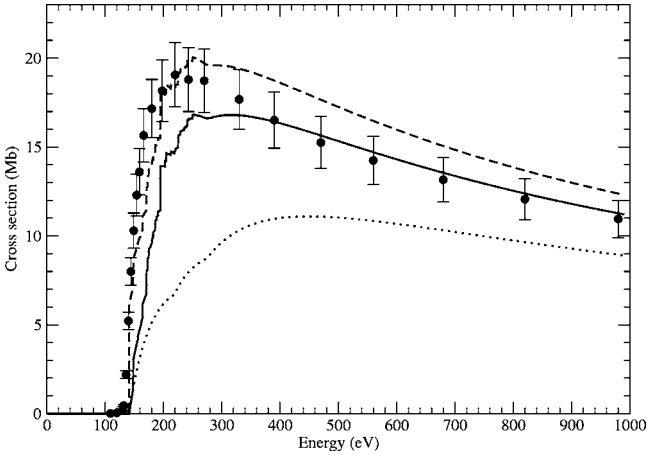

FIG. 10. Electron-impact single-ionization cross section for Pb^{8+}, which has a ground configuration of $5d^6$. The dotted line gives the total CADW-DI cross section from the ground configuration, and the solid line gives the total CADW-DI plus the total CADW-EA cross section for the ground configuration. The dashed line shows the total direct ionization plus the total excitation autoionization with the excitation from the $5d \rightarrow 5f$ subshells included. The solid circles show the experimental results.

and excitation autoionization via core excitation of the $5p$ and $5s$ subshells to the $5p^5 5d^7 nl$ and $5s5p^6 5d^7 nl$ configurations, respectively, where $5 \leqslant n \leqslant 8$ and $0 \leqslant l \leqslant 3$. Table I shows the direct-ionization potentials for Pb^{7+}. For Pb^{7+} we expect any metastable terms to be contained within the ground configuration.

From Fig. 9 one can see that there is reasonable agreement between theory and experiment. The theory results are in excellent agreement up to the peak of the cross section and then trend slightly high at higher energy. It can be seen from Table I that the configuration-average ionization potential of the $4f$ subshell is only slightly below the double-ionization potential for Pb^{7+}. Thus, it may be that the direct ionization of the $4f$ subshell actually produces levels which are in fact double autoionizing, leading to a reduction in the theoretical cross section at higher energies.

H. Pb^{8+}

The theoretical and experimental results for Pb^{8+} are shown in Fig. 10. Pb^{8+} has a ground configuration of $5d^6$. We include direct ionization of the $5d$, $5p$, $5s$, and $4f$ subshells and excitation autoionization via core excitation of the $5p$ and $5s$ subshells to the $5p^5 5d^6 nl$ and $5s5p^6 5d^6 nl$ configurations, respectively, where $5 \leqslant n \leqslant 8$ and $0 \leqslant l \leqslant 3$. Table I shows the direct-ionization potentials for Pb^{8+}. The results for Pb^{8+} lie slightly below those of experiment at the peak of the cross section, but agree well at higher energy. The presence of autoionizing configurations just below the configuration-average ionization threshold is likely to be contributing to this discrepancy. Note that if we include the contribution from excitation of the $5p$ subshell to the $5f$ subshell, we get much better agreement near threshold. Due to the large number of levels in this $5s^2 5p^5 5d^6 5f$ configuration, it was not possible to calculate excitation to this configuration in the level-resolved picture.

I. Pb^{9+}

The theoretical and experimental results for Pb^{9+} are shown in Fig. 11. Pb^{9+} has a ground configuration of $5d^5$. With the large number of terms in this ground configuration,

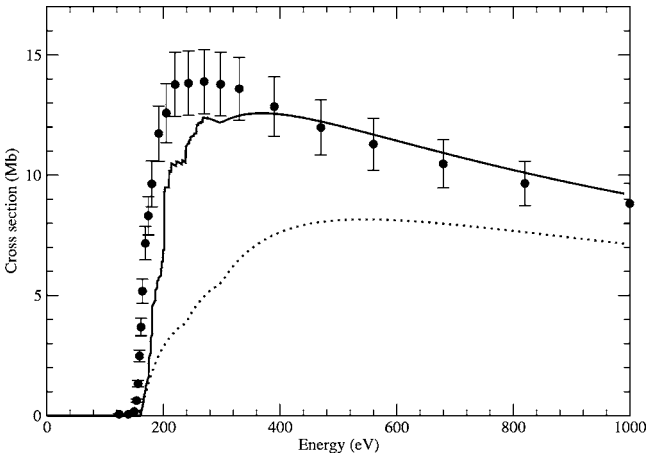

FIG. 11. Electron-impact single-ionization cross section for Pb^{9+}, which has a ground configuration of $5d^5$. The dotted line gives the total CADW-DI cross section from the ground configuration, and the solid line gives the total CADW-DI plus the total CADW-EA cross section for the ground configuration. The solid circles show the experimental results.

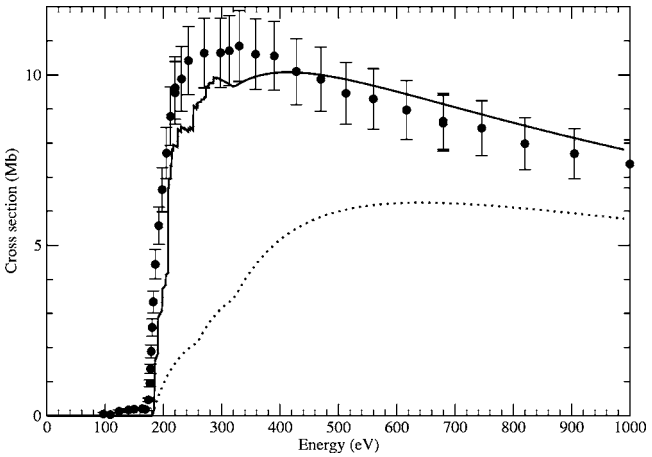

FIG. 12. Electron-impact single-ionization cross section for Pb^{10+}, which has a ground configuration of $5d^4$. The dotted line gives the total CADW-DI cross section from the ground configuration, and the solid line gives the total CADW-DI plus the total CADW-EA cross section for the ground configuration. The solid circles show the experimental results.

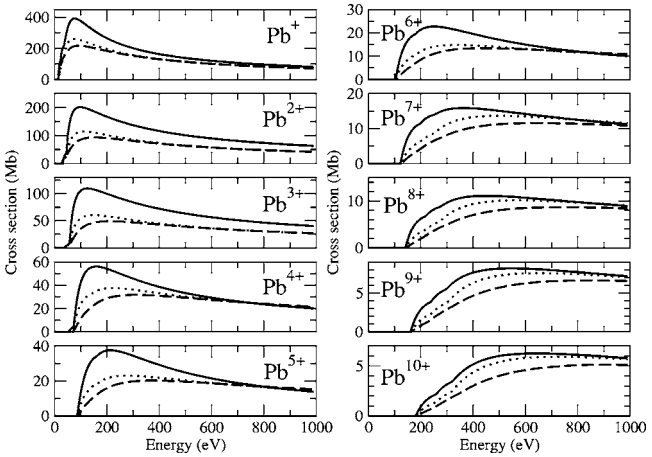

FIG. 13. Theoretical electron-impact single-ionization cross section for the ground configurations of the first ten ion stages of Pb, showing the CADW-DI (solid line), Lotz (dotted line), and BEB (dashed line) results.

we do not expect the presence of significant metastable terms in the first excited configuration. In the theoretical calculations we include direct ionization from the $5d$, $5p$, $5s$, and $4f$ subshells and excitation autoionization from core excitations of the $5p$ and $5s$ subshells to the $5p^5 5d^5 nl$ and $5s5p^6 5d^5 nl$ configurations, respectively, where $5 \leqslant n \leqslant 8$ and $0 \leqslant l \leqslant 3$. Table I shows the direct-ionization potentials for Pb^{9+}. There is excellent agreement between the CADW theory results and experiment at higher energies, and there is reasonable agreement near threshold.

J. Pb^{10+}

The theoretical and experimental results for Pb^{10+} are shown in Fig. 12. Pb^{10+} has a ground configuration of $5d^4$. In the theory results we include direct ionization from the $5d$, $5p$, $5s$, and $4f$ subshells and excitation autoionization via core excitation of the $5p$ and $5s$ subshells to the $5p^5 5d^4 nl$ and $5s5p^6 5d^4 nl$ configurations, respectively, where $5 \leqslant n \leqslant 8$ and $0 \leqslant l \leqslant 3$. Table I shows the direct-ionization potentials for Pb^{10+}. There is excellent agreement between the CADW theory and experiment, except just at the peak of the cross section, where theory is slightly below experiment.

K. Other methods for calculating the direct ionization

There are various semiempirical methods which are often used to calculate the direct-ionization cross section. It is thus instructive to compare these with the results from our calculations. We look at the BEB method [11,12] and the Lotz method [10]. Neither of these methods accounts for excitation autoionization, so we compare them with the direct-ionization cross section from distorted-wave theory. We find this more instructive than comparing with the experimental measurements, because, especially for the low ion stages, it is not possible to separate the direct and indirect cross sections from the experiment without relying on theory.

The cross section results for these semiempirical methods are easily worked out from Eqs. (7) and (8), with the results being shown for the ground configurations of all ion stages in Fig. 13. The BEB and Lotz cross sections are always smaller than the distorted-wave results for the direct ionization. We note that the BEB results are also consistently smaller than the Lotz results. Further inspection of Fig. 13 reveals the following trends. Both the Lotz and BEB results approach the CADW direct-ionization results at higher energy. Also, with increasing ion stage, both the Lotz and BEB methods are becoming progressively closer to the CADW direct ionization results, with the Lotz results approaching the CADW direct-ionization results faster than the BEB results do.

V. SUMMARY

Recent experimental measurements for electron impact single ionization of Pb^+ through to Pb^{10+} have been compared with configuration-average distorted-wave theory and level-resolved distorted-wave theory. Distorted-wave theory overestimates the total cross section for ion stages Pb^+, Pb^{2+}, and Pb^{3+}. However, for the higher ion stages, the agreement is very good. We detect the presence of a metastable fraction in ion stages Pb^{2+} through to Pb^{6+}. Excitation autoionization is clearly important for all of the ion stages studied here.

Level-resolved distorted-wave calculations of the dominant excitations reduce the total theoretical cross section slightly for Pb^{3+}, but do not significantly change the CADW results for Pb^+, Pb^{2+}, Pb^{4+}, and Pb^{5+}. For the higher ion stages there were too many levels in the excited configurations (with open p, d, and sometimes f subshells) for level-resolved calculations to be performed.

As part of the work resulting from this paper, we intend to look at nonperturbative means of calculating the direct-ionization cross section for complex, near-neutral species. Work is already underway for Mo^+ electron-impact ionization calculations. We also intend to extend the work here to other heavy species.

ACKNOWLEDGMENTS

This work was supported by a grant from the Office of Fusion Science by the U.S. Department of Energy. Support by the Deutsche Forschungsgemeinschaft (DFG), Bonn-Bad Godesberg, is gratefully acknowledged.

[1] ITER Physics Basis, Nucl. Fusion **39**, 2137 (1999); Plasma Phys. Controlled Fusion **44**, B323 (2002).
[2] H. P. Summers, N. R. Badnell, M. G. O'Mullane, A. D. Whiteford, R. Bingham, B. J. Kellet, J. Lang, K. H. Behringer, U. Fantz, K.-D. Zastrow, S. D. Loch, M. S. Pindzola, D. C. Griffin, and C. P. Ballance, Plasma Phys. Controlled Fusion **44**, B323 (2002).
[3] M. G. O'Mullane, H. P. Summers, A. D. Whiteford, R. Barnsley, I. H. Coffey, G. Counsell, and S. D. Loch, Rev. Sci. Instrum. **74**, 2080 (2003).
[4] M. S. Pindzola, D. C. Griffin, and C. Bottcher, in *Atomic Processes in Electron-ion and Ion-ion Collisions*, Vol. 145 of *NATO Advanced Study Institute, Series B: Physics*, edited by F. Brouillard (Plenum, New York, 1986).
[5] M. S. Pindzola, D. C. Griffin, and C. Bottcher, Phys. Rev. A **34**, 3668 (1986).
[6] M. S. Pindzola, D. C. Griffin, C. Bottcher, S. M. Younger, and T. H. Hunter, Nucl. Fusion Suppl.21 (1987).
[7] D. Hathiramani, K. Aichele, G. Hofmann, M. Steidl, M. Stenke, R. Völpel, E. Salzborn, M. S. Pindzola, J. A. Shaw, D. C. Griffin, and N. R. Badnell, Phys. Rev. A **54**, 587 (1996).
[8] S. D. Loch, M. S. Pindzola, C. P. Ballance, D. C. Griffin, D. M. Mitnik, N. R. Badnell, M. G. O'Mullane, H. P. Summers, and A. D. Whiteford, Phys. Rev. A **66**, 052708 (2002).
[9] S. D. Loch, M. S. Pindzola, N. R. Badnell, F. Scheuermann, K. Kramer, K. Huber, and E. Salzborn, Phys. Rev. A **70**, 052714 (2004).
[10] W. Lotz, Z. Phys. **216**, 241 (1968).
[11] Y.-K. Kim and M. E. Rudd, Phys. Rev. A **50**, 3954 (1994).
[12] Y.-K. Kim and P. M. Stone, Phys. Rev. A **64**, 052707 (2001).
[13] V. M. Povyshev, A. A. Sadovoy, V. P. Shevelko, G. D. Shirkov, E. G. Vasina, and V. V. Vatulin, Jt. Inst. Nucl. Invest., Dubna, USSR, Rep. JINR **E9**, 148 (2001).
[14] M. S. Pindzola and D. C. Griffin, Phys. Rev. A **46**, 2486 (1992).
[15] J. Colgan and M. S. Pindzola, Phys. Rev. A **66**, 062707 (2002).
[16] J. Colgan, M. S. Pindzola, D. M. Mitnik, and D. C. Griffin, Phys. Rev. A **63**, 062709 (2005).
[17] S. D. Loch, M. Witthoeft, M. S. Pindzola, I. Bray, D. V. Fursa, M. Fogle, R. Schuch, P. Glans, C. P. Ballance, and D. C. Griffin, Phys. Rev. A **71**, 012716 (2005).
[18] J. Jacobi, H. Knopp, S. Schippers, A. Müller, S. D. Loch, M. Witthoeft, M. S. Pindzola, and C. P. Ballance, Phys. Rev. A **70**, 042717 (2004).
[19] M. S. Pindzola, T. W. Gorczyca, N. R. Badnell, D. C. Griffin, M. Stenke, G. Hofmann, B. Weissbecker, K. Tinschert, E. Salzborn, A. Müller, and G. H. Dunn, Phys. Rev. A **49**, 933 (1994).
[20] D. C. Griffin, C. Bottcher, and M. S. Pindzola, Phys. Rev. A **25**, 1374 (1982).
[21] K. Tinschert, A. Müller, G. Hofmann, K. Huber, R. Becker, D. C. Gregory, and E. Salzborn, J. Phys. B **22**, 531 (1989).
[22] G. Hofmann, A. Müller, K. Tinschert, and E. Salzborn, Z. Phys. D: At., Mol. Clusters **16**, 113 (1990).
[23] F. Brötz, Dissertation, http://geb.uni-giessen.de/geb/volltexte/2000/263/.
[24] A. Müller, K. Tinschert, Ch. Achenbach, E. Salzborn, R. Becker, and M. S. Pindzola, Phys. Rev. Lett. **54**, 414 (1985); J. Phys. B **21**, 3253 (1988).
[25] R. Becker, A. Müller, Ch. Achenbach, K. Tinschert, and E. Salzborn, Nucl. Instrum. Methods Phys. Res. B **9**, 385 (1985).